

# Persistence and origin of the lunar core dynamo

Clément Suavet<sup>a,1</sup>, Benjamin P. Weiss<sup>a</sup>, William S. Cassata<sup>b</sup>, David L. Shuster<sup>c,d</sup>, Jérôme Gattacceca<sup>a,e</sup>, Lindsey Chan<sup>f</sup>, Ian Garrick-Bethell<sup>f,g</sup>, James W. Head<sup>h</sup>, Timothy L. Grove<sup>a</sup>, and Michael D. Fuller<sup>i</sup>

<sup>a</sup>Department of Earth, Atmospheric, and Planetary Sciences, Massachusetts Institute of Technology, Cambridge, MA 02139; <sup>b</sup>Chemical Sciences Division, Lawrence Livermore National Laboratory, Livermore, CA 94550; <sup>c</sup>Department of Earth and Planetary Science, University of California, Berkeley, CA 94720; <sup>d</sup>Berkeley Geochronology Center, Berkeley, CA 94709; <sup>e</sup>Centre Européen de Recherche et d'Enseignement des Géosciences de l'Environnement, Centre National de la Recherche Scientifique, Université Aix-Marseille 3, 13545 Aix-en-Provence, France; <sup>f</sup>Department of Earth and Planetary Sciences, University of California, Santa Cruz, CA 95064; <sup>g</sup>School of Space Research, Kyung Hee University, Yongin 446-701, South Korea; <sup>h</sup>Department of Geological Sciences, Brown University, Providence, RI 02912; and <sup>i</sup>Hawai'i Institute of Geophysics and Planetology, University of Hawaii at Manoa, Honolulu, HI 96822

Edited by Neta A. Bahcall, Princeton University, Princeton, NJ, and approved April 16, 2013 (received for review January 22, 2013)

**The lifetime of the ancient lunar core dynamo has implications for its power source and the mechanism of field generation. Here, we report analyses of two 3.56-Gy-old mare basalts demonstrating that they were magnetized in a stable and surprisingly intense dynamo magnetic field of at least  $\sim 13 \mu\text{T}$ . These data extend the known lifetime of the lunar dynamo by  $\sim 160$  My and indicate that the field was likely continuously active until well after the final large basin-forming impact. This likely excludes impact-driven changes in rotation rate as the source of the dynamo at this time in lunar history. Rather, our results require a persistent power source like precession of the lunar mantle or a compositional convection dynamo.**

high-K mare basalts | paleomagnetism

The existence of a global planetary magnetic field provides evidence of an advecting liquid core. Although the Moon does not have a global field today, lunar crustal magnetism and paleomagnetism in returned samples provide evidence of an ancient lunar dynamo (1, 2). Laser ranging experiments (3) and reanalysis of Apollo-era seismic data (4, 5) indicate that the Moon currently has a small ( $\sim 330$  km) partially molten metallic core. Recent paleomagnetic studies of slowly cooled, unshocked samples demonstrate that the Moon had a core dynamo at 4.2 Ga (6) and 3.7 Ga (7). However, the subsequent history of the lunar dynamo is largely unknown.

Determining the lifetime of the lunar dynamo would constrain the nature of its power source and the mechanism of magnetic field generation. Models of core thermal convection have found that a lunar dynamo can only unambiguously persist for as late as 4.1 Ga, well before the youngest current evidence for the magnetic field at 3.7 Ga (7). Although a compositional convection dynamo driven by the crystallization of the core is also possible, the lifetime of such a dynamo is currently unclear. This has motivated alternative models that use precession (8, 9) and/or basin-forming impacts (10) to power the dynamo mechanically via differential motion between the liquid core and rocky mantle. Precession appears to be capable of powering a dynamo until as late as  $\sim 1.8$ – $2.7$  Ga (9). By comparison, a dynamo driven by impact-induced unlocking from synchronous rotation could likely be active only when basin-forming impacts occurred, before or during the Early Imbrian epoch ( $\geq \sim 3.72$  Ga). Therefore, these two mechanisms could potentially be distinguished using measurements of the lunar magnetic field after this time.

Some Apollo-era paleomagnetic studies argued that the termination of the lunar dynamo occurred before the eruption of the Apollo 11 high-K basalts at  $\sim 3.6$  Ga (11), whereas others suggested that the dynamo persisted but slowly decayed until at least  $\sim 3.2$  Ga (12). Two Apollo 11 samples, mare basalts 10017 and 10049, provided contrasting results that were central to this debate. Analyses of 10017 (13–16) identified one of the most stable natural remanent magnetization (NRM) records identified in any lunar sample. However, the presence of Johnson Space Center (JSC) saw marks on some subsamples and what was perceived to be a wide range of paleointensities ( $\sim 40$ – $90 \mu\text{T}$ ) led these investigators to exclude

10017 as a constraint on the lunar dynamo. Instead, these authors relied on their analyses of 10049, whose subsamples were found to carry a unidirectional magnetization (17) with a seemingly weak paleointensity ( $4$ – $10 \mu\text{T}$ ). However, our reanalysis of their data with modern multicomponent methods yields paleointensities up to  $\sim 30 \mu\text{T}$  (*SI Appendix*).

A recent paleomagnetic study found that lunar samples with ages of 3.3 Ga and in the range 3.7–3.94 Ga may have recorded a field of several tens of microteslas (18). In this study, only one sample (12002, which has an age of 3.3 Ga) was younger than Apollo high-K basalts. However, the nature of its paleomagnetic record is currently ambiguous: Its NRM does not trend toward the origin during alternating field (AF) demagnetization, its remanent magnetization derivative (REM') paleointensity (19) varies by nearly an order of magnitude throughout the demagnetization, the sample was measured while encased in a container whose moment was similar to the demagnetized sample, and no mutually oriented subsamples were measured.

## Samples

Mare basalts 10017 and 10049 are fine-grained, high-K ilmenite basalts of petrological group A (20, 21). Their major phases are pyroxene (50.6 vol % and 51.3%, respectively), plagioclase (23.6 vol. % and 24.5%, respectively), and ilmenite (15.1 vol % and 14.1%, respectively), and minor mesostasis includes high-K glass (21) (*SI Appendix*). These basalts erupted at  $\sim 3.56$  Ga and form the present surface of most of the southwest portion of Mare Tranquillitatis. The collected rock samples are thought to have been excavated by the impact that formed West Crater  $\sim 100$  Ma (21),  $\sim 0.5$  km from the Apollo 11 landing site.

We observed similar mineral assemblages and compositions as those previously described for these samples (21). Our electron microprobe analyses of metal in 10017,62 and 10049,40 found that it has a composition of nearly pure metallic iron ( $\text{Fe}_{1-x}\text{Ni}_x$  with  $x < 0.02$ ) and is typically intergrown with troilite (*SI Appendix*). Because the high-temperature taenite phase ( $\gamma\text{-Fe}$ ) with this bulk composition transforms fully to kamacite at  $912^\circ\text{C}$ , which is above Curie temperature of  $780^\circ\text{C}$  (22), the kamacite in these rocks should have acquired a pure thermoremanent magnetization (TRM) during primary cooling rather than the thermochemical remanent magnetization that forms when  $x > 0.03$  (23). Rock magnetic experiments (*SI Appendix*) indicate that the kamacite grain size is in the multidomain range for both 10017 and 10049.

Author contributions: C.S., B.P.W., and M.D.F. designed research; C.S., W.S.C., D.L.S., J.G., L.C., I.G.-B., J.W.H., and T.L.G. performed research; W.S.C., D.L.S., and J.G. contributed new reagents/analytic tools; C.S., W.S.C., and D.L.S. analyzed data; and C.S. and B.P.W. wrote the paper.

The authors declare no conflict of interest.

This article is a PNAS Direct Submission.

<sup>1</sup>To whom correspondence should be addressed. E-mail: csuavet@mit.edu.

This article contains supporting information online at [www.pnas.org/lookup/suppl/doi:10.1073/pnas.1300341110/-DCSupplemental](http://www.pnas.org/lookup/suppl/doi:10.1073/pnas.1300341110/-DCSupplemental).

To constrain the samples' cooling rates below 1,100 °C, we measured the width of the largest plagioclase lath perpendicular to the (010) faces following the method used by Grove and Beaty (20) (*SI Appendix*, Section 9). Our measured values of 550  $\mu\text{m}$  and 120  $\mu\text{m}$  indicate cooling rates of  $\sim 0.03$  °C·h<sup>-1</sup> and  $\sim 0.43$  °C·h<sup>-1</sup> for 10017 and 10049, respectively, which correspond to cooling times from the Curie point to ambient lunar surface temperatures of  $\sim 10^3$  d and  $\sim 10^2$  d, respectively. Because these samples are antiophitic, these are likely minimum estimates of the cooling timescale (20). These time scales are much longer than the expected 1-d maximum lifetime of fields generated by basin-forming impacts (24). Therefore, any primary magnetization in these samples is likely a record of a temporally stable field like that expected for a core dynamo. Furthermore, we observed no petrographic evidence for shock (peak pressure <5 GPa), such as plagioclase fracturing, mechanical twinning, or alteration to maskelynite (*SI Appendix*). Mare basalts 10017 and 10049 are therefore ideal samples for testing the lunar dynamo hypothesis late in lunar history.

### NRM

We carried out AF demagnetization up to 85–290 mT on eight mutually oriented subsamples of 10017,378 and on three mutually oriented subsamples of 10049,102 (all samples without JSC saw cut faces). Because 10017 and 10049 were collected as regolith float by the Apollo astronauts, they are not mutually oriented,

although their individual subsamples are mutually oriented with respect to their parent rock. We found that the subsamples had NRM intensities of  $5.5 \times 10^{-6}$ – $3.5 \times 10^{-5}$  Am<sup>2</sup>·kg<sup>-1</sup> for 10017 and  $1.1 \times 10^{-5}$  to  $2.3 \times 10^{-5}$  Am<sup>2</sup>·kg<sup>-1</sup> for 10049. All demagnetized samples were observed to have two components of magnetization (Fig. 1, Table 1, and *SI Appendix*). All samples had a low coercivity (LC) and a high coercivity (HC) component. The LC component was removed by AF demagnetization up to somewhere between 9 and 20 mT for subsamples of 10017, with the exception of subsample 378-10, for which the LC and HC components demagnetized concurrently up to several tens of microteslas. The LC component was removed by AF demagnetization between 4 and 11.5 mT for subsamples of 10049. For all samples (with the exception of subsample 378-10), these values are lower than or comparable to those observed by previous studies: The LC component was removed at  $\sim 50$  mT for 10017 (16) and at  $\sim 20$  mT for 10049 (17). The LC component is inconsistent in direction between subsamples (Fig. 2) and decays like an isothermal remanent magnetization (IRM) during AF demagnetization (*SI Appendix*). The ratio of the LC component to an IRM (19) ranges between 0.026 and 0.083 over its coercivity range. These results indicate that the LC components in each basalt are likely to be overprints acquired in a strong artificial field during transportation (25) or preparation of the samples at the JSC.

The HC component was observed to decay throughout the demagnetization up to at least 85 mT for all subsamples. Stepwise demagnetization was carried out up to even higher fields for samples 10017,378-2, 10017,378-3, 10017,378-8, and 10049,102-2 (*SI Appendix*). We found that subsample 378-3 had a directionally stable HC magnetization that continued to decay in intensity up to 120 mT, beyond which it remained directionally stable but without further decay up to 290 mT [likely due to anhysteretic remanent magnetization (ARM) noise]. We found that the HC magnetization in subsample 378-2 was stable in direction and continued to decay in intensity up to 120 mT, at which point the sample had completely demagnetized (i.e., became directionally unstable). Subsample 378-8 was stable in direction and decaying in intensity up to 110 mT, beyond which it remained relatively stable in direction with a superposed random component, again likely due to ARM noise. Subsample 102-2 was stable in direction and decaying in intensity up to 290 mT, whereas subsamples 102-1 and 102-3 were directionally stable and decaying in intensity up to at least 85 mT. The HC components are unidirectional within both 10017,378 and 10049,102. The maximum angle between the HC directions is 18° for 10017 and 8° for 10049. For 10017, the Fisher mean direction 95% confidence angle is 6.0° and the Fisher precision parameter is  $k = 153$  (number of samples,  $n = 6$ ). For 10049, the Fisher mean direction 95% confidence angle is 6.9° and the Fisher precision parameter is  $k = 478$  ( $n = 3$ ). Given the orientation uncertainty of  $\sim 5$ – $10^\circ$  and maximum angular deviation (MAD) values in the range of 2.8– $10.0^\circ$  for 10017 and 5.2– $10.6^\circ$  for 10049, the HC directions are therefore indistinguishable from one another within both samples. In the absence of a statistical method to estimate whether a magnetization component is origin-trending with a confidence interval, we compared the angle between the best-fitting line through the data and the line connecting the origin with the center of mass of the data [deviation angle (DANG) (26)] with the MAD. We found a DANG < MAD for all HC components for both basalt samples, suggesting that the magnetizations are origin-trending, and are therefore the characteristic magnetizations.

To determine whether the NRMs of 10017 and 10049 were contaminated by viscous remanent magnetization (VRM) acquired during their 40-y exposure to the geomagnetic field since return to Earth, and how much of this VRM subsequently decayed during storage in our shielded room before our NRM measurements, we conducted VRM acquisition and decay experiments (*SI Appendix*). For 10017, we found that the residual VRM would be  $9.4 \times 10^{-11}$

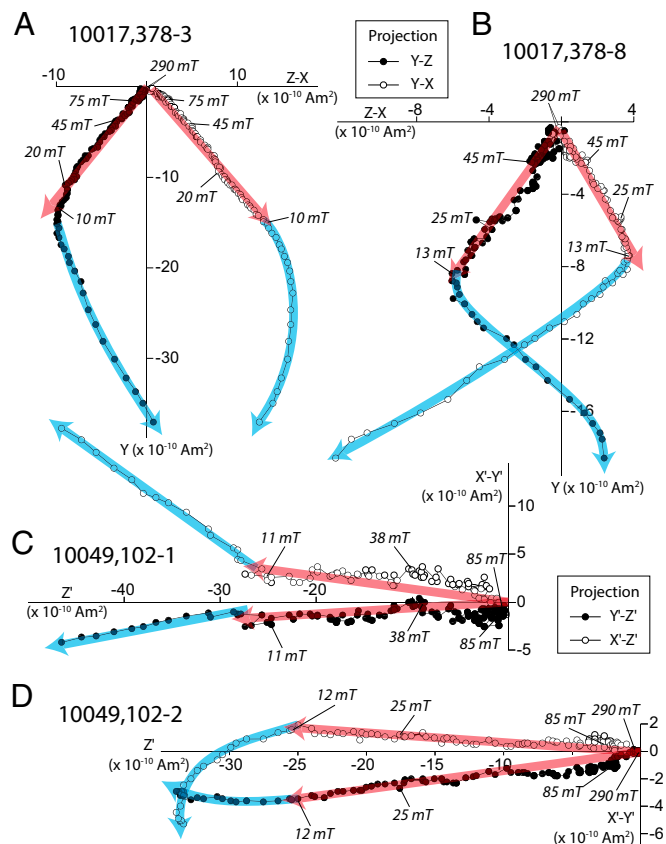


**Fig. 1.** NRM in mare basalts 10017 and 10049. Shown is a 2D projection of the NRM vectors of subsamples 10017,378-3; 10017,378-8; 10049,102-1; and 10049,102-2 during AF demagnetization. Solid (●) [open (○)] circles represent end points of magnetization projected onto the Y-Z (X-Y) planes for 10017 and onto the Y'-Z' (X'-Z') planes for 10049. Peak fields for selected AF steps are labeled in microteslas. Red arrows denote HC component directions determined from principal component analyses. Subsample 10017,378-3 (A); subsample 10017,378-8 (B); subsample 10049,102-1 (C); and subsample 10049,102-2 (D).

**Table 1. Summary of LC and HC components for subsamples from 10017,378 and 10049,102 obtained with principal component analysis**

Sample	Component	AF range, mT	Type	Dec., Inc.; °	MAD, °	DANG, °	N	Paleointensity, $\mu\text{T}$		
								ARM, 50 $\mu\text{T}$	ARM, 100 $\mu\text{T}$	IRM
10017,378-1	LC	NRM-10	L	52.0, -30.9	2.3		19			
	HC	10.5-85	AL	310.6, -44.0	4.1/4.8	3.5	90			
10017,378-2	LC	NRM-9	L	322.0, 43.5	23.3		17			
	HC	9.5-120	AL	310.0, -35.6	2.8/3.6	1.3	102	83.5 $\pm$ 1.2	80.6 $\pm$ 0.8	95.1 $\pm$ 4.6
10017,378-3	LC	NRM-10	L	271.3, 25.4	7.9		19			
	HC	10.5-290	AL	312.6, -30.1	4.8/5.7	3.0	101	78.2 $\pm$ 1.7	76.7 $\pm$ 1.1	82.9 $\pm$ 1.6
10017,378-6	LC	NRM-20	L	232.6, 25.6	7.8		39			
	HC	20.5-85	AL	303.6, -34.0	7.0/12.3	1.9	70			
10017,378-7	LC	NRM-10	L	186.8, 16.0	3.0		19			
	HC	10.5-85	AL	308.7, -35.4	3.9/5.7	2.3	90	64.9 $\pm$ 1.2	55.5 $\pm$ 0.8	61.9 $\pm$ 3.0
10017,378-8	LC	NRM-13	L	213.1, 26.7	5.2		25			
	HC	13.5-110	AL	297.1, -28.8	10.0/14.0	5.8	95	50.5 $\pm$ 1.5	47.2 $\pm$ 1.6	43.2 $\pm$ 2.3
10017,378-10	LC	NRM-20	L	219.2, -24.1	7.3		39			
	HC	20-180	AL	271.7, -51.4	3.8/4.9	2.5*	128			
	HC	20-180	C	78.1, -37.9	18.2		128			
10017,378-11	All	NRM-180	C	95.3, -37.6	15.7		166			
	LC	NRM-15	L	243.3, -58.6	8.2		30			
10049,102-1	HC	15-180	AL	313.5, -40.1	3.0/4.2	4.1*	137			
	LC	NRM-10.5	L	353.1, -53.3	5.7		20			
10049,102-2	HC	11-85	AL	332.5, -77.9	10.6/13.7	4.7	89	69.7 $\pm$ 5.3	86.3 $\pm$ 4.6	95.2 $\pm$ 4.3
	LC	NRM-11.5	L	175.2, -51.2	12.6		22			
10049,102-3	HC	12-290	AL	294.2, -80.2	5.2/6.0	2.9	96	55.2 $\pm$ 1.3	49.3 $\pm$ 1.0	59.1 $\pm$ 3.2
	LC	NRM-4	L	268.6, -1.1	23.8		3			
	HC	6-85	AL	339.7, -79.1	6.6/9.1	7.6	20			

The first column gives the subsample name and component name; the second column gives the magnetization component; the third column gives the range of AF steps used for the fit; the fourth column gives the fit type (AL, line anchored to the origin; C, circle fit forced through the origin, poles reported; L, line); the fifth column gives the declination (Dec.) and inclination (Inc.) of the fit direction (for line fits) or great circle pole (for circle fits); the sixth column gives the MAD of the component forced through the origin/not forced through the origin; the seventh column gives the DANG; and the eighth column gives the number of AF steps used in fit ( $N$ ). The last three columns give paleointensities: ARM paleointensity (in microteslas) = (NRM lost)/(ARM lost)/ $f \times$  [bias field (in microteslas)]  $\times$  anisotropy correction factor, IRM paleointensity (in microteslas) = (NRM lost)/(IRM lost)  $\times a \times$  anisotropy correction factor. We used  $f = 1.34$  and  $a = 3,000$ . Uncertainties on each paleointensity value are formal 95% confidence intervals on the slope fit using the Student  $t$  test (31) and do not include the factor of  $\sim 3$ – $5$  uncertainty associated with the unknown ratios of ARM and IRM to TRM.

\*DANG calculated using first point of fit.

$\text{Am}^2$ , equivalent to only 2.4% of the observed initial NRM. For 10049, we found that the residual VRM would be  $9.3 \times 10^{-11} \text{ Am}^2$ , equivalent to only 2.7% of the initial NRM. Therefore, neither the

LC nor HC components of 10017 and 10049 are likely to be VRM-acquired in the Earth's magnetic field.

Although our petrographic observations exclude shocks with pressures  $>5$  GPa, even shocks with lower peak pressures could produce magnetization if a field were present. To investigate this possibility, we conducted pressure remanent magnetization (PRM) acquisition experiments (*SI Appendix*) for subsamples 378-3 and 102-1 following the method used by Gattacceca (27). Like previous such studies of lunar rocks (27), we found that PRM was acquired dominantly by LC grains ( $< \sim 30$ – $40$  mT) with even the 2.0-GPa PRM significantly softer than the NRM (*SI Appendix*). This suggests that neither the LC nor HC components are likely shock remanent magnetizations (SRM). We found that a 1-mT field and a 2-mT field would have been necessary to produce the LC and HC components of 378-3, respectively. Similarly, a 0.1-mT field and a 0.3-mT field would have been necessary to produce the LC and HC components of 102-1, respectively. Such fields are well above theoretical estimates of maximum dynamo fields for the Moon and at the upper end of predicted impact-generated fields (e.g., refs. 28, 29). Therefore, these field values provide further evidence against an SRM origin for either NRM component.

We conducted AF demagnetization of laboratory-induced magnetizations and compared them with that of the NRM. The HC component in each rock demagnetizes like an ARM [an analog of TRM (30)] and unlike either a PRM or an IRM (*SI Appendix*).

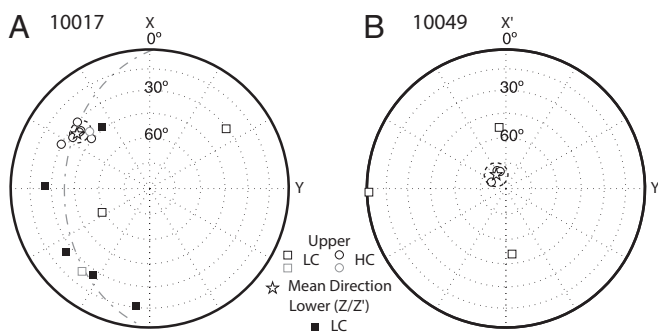


**Fig. 2.** Equal area stereographic projection of NRM component fits. Circles denote HC directions (primary magnetization) for each subsample, and squares denote LC directions (overprint). The stars are the Fisher mean HC direction from principal component analyses, with surrounding dashed ellipses indicating 95% formal confidence intervals on mean directions (not accounting for additional  $\sim 3$ – $5^\circ$  mutual orientation uncertainty). (A) Sample 10017,378. Black and gray symbols correspond to samples measured at the Massachusetts Institute of Technology and University of California, Santa Cruz, respectively. The dashed great circle denotes a circle fit forced through the origin for the HC data of subsample 10. (B) Sample 10049,102.



Therefore, the HC components of 10017 and 10049 are likely TRMs acquired during cooling in a stable field on the Moon.

### Paleointensity

The HC components of 10017,378 yielded anisotropy-corrected paleointensities ranging between 47 and 84  $\mu\text{T}$  from the ARM method and between 43 and 95  $\mu\text{T}$  from the IRM method; 10049,102 yielded anisotropy-corrected HC component paleointensities ranging between 49.3 and 86.3  $\mu\text{T}$  from the ARM method and between 59.1 and 95.2  $\mu\text{T}$  from the IRM method (Table 1 and *SI Appendix*). The range of variability between subsamples is expected, given the uncertainty in the calibration factors for these methods. Furthermore, the similarity between the ARM and IRM values gives confidence that each method is producing relatively accurate results. Given that each individual paleointensity is uncertain by a factor of 3–5, the multispecimen mean values should be significantly less uncertain than this factor. The average values for the ARM method are  $67 \pm 15 \mu\text{T}$  for 10017 and  $65 \pm 14 \mu\text{T}$  for 10049 [uncertainties are formal 95% confidence intervals on the slope fit using the Student  $t$  test (31) and do not include the factor of  $\sim 3$ –5 uncertainty associated with the unknown ratios of ARM and IRM to TRM]. The average values for the IRM method are  $71 \pm 21 \mu\text{T}$  for 10017 and  $77 \pm 18 \mu\text{T}$  for 10049 (uncertainties on mean values are observed

1 SD from multiple samples). These paleointensities are indistinguishable within the uncertainty and give a mean value for all experiments on both samples of  $69 \pm 16 \mu\text{T}$ , which corresponds to a very conservative minimum paleofield of  $\sim 13 \mu\text{T}$ . These values are also within error of the paleointensity inferred at 3.7 Ga from mare basalt 10020 (7) and consistent with values recently obtained for other samples with crystallization ages from 3.7 to 3.94 Ga (18) (although the age and origin of the magnetization in the latter samples are not well constrained). These paleointensities are higher than previous estimates for 10049, likely due to lack of complete NRM demagnetization in these earlier studies (*SI Appendix*).

### Thermochronology

The 3.56-Ga crystallization ages of 10017 and 10049 place an upper limit on the time at which they acquired their magnetization. It is possible that the magnetization of these rocks could have been acquired or reset during thermal excursions following their formation. Although the lack of shock features in these rocks precludes direct shock heating, they could have experienced temperature excursions from burial in a hot ejecta blanket or nearby volcanic activity. To assess this possibility, we conducted  $^{40}\text{Ar}/^{39}\text{Ar}$  and  $^{38}\text{Ar}/^{37}\text{Ar}$  thermochronometry on two whole-rock subsamples of 10017 and 10049 (Fig. 3 and *SI Appendix*).

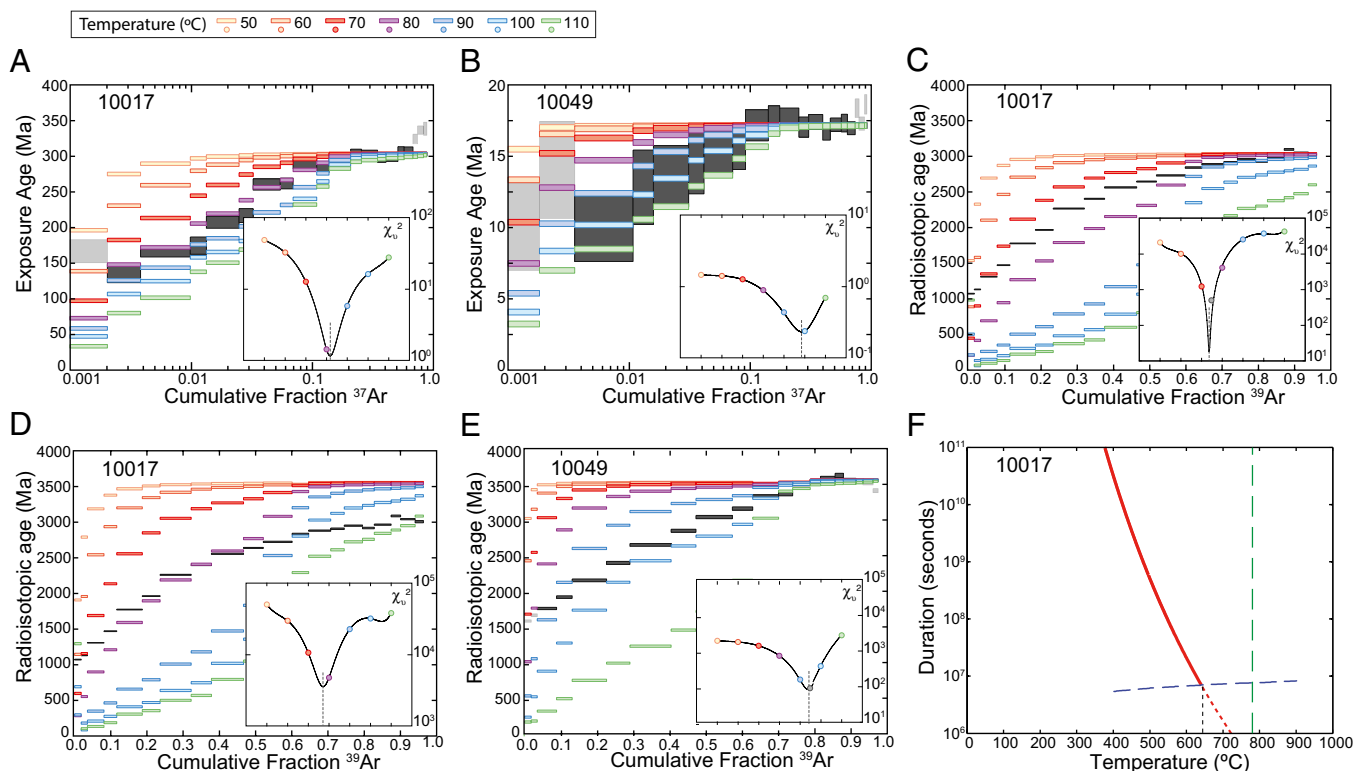


**Fig. 3.** Radiogenic  $^{40}\text{Ar}$  and cosmogenic  $^{38}\text{Ar}$  thermochronometry of whole-rock mare basalts 10017 and 10049. Production and diffusion of  $^{38}\text{Ar}_{\text{cos}}$  for 10017 (A) and 10049 (B). The observed exposure ages  $\pm 1$  SD (gray boxes) are plotted against the cumulative release fraction of  $^{37}\text{Ar}$ .  $^{38}\text{Ar}_{\text{cos}}$  was produced in situ while the rocks were exposed at the surface of the Moon. The colored steps are model release spectra calculated using the multiphase, multidomain model (model parameters are provided in *SI Appendix*) for the production and diffusion of  $^{38}\text{Ar}_{\text{cos}}$ , assuming the rocks were subjected to various constant effective daytime temperatures ranging from 50 to 110  $^{\circ}\text{C}$  during the last 303.1 Ma for 10017 or during the last 17.2 Ma for 10049 (i.e.,  $^{38}\text{Ar}_{\text{cos}}$  is produced continuously over this duration, whereas diffusion occurs only over half of this period during elevated daytime temperatures). (Insets) Reduced  $\chi^2$  fit statistic for each model, identifying  $\sim 80^{\circ}\text{C}$  as the best-fit effective mean temperature for 10017 and  $\sim 95^{\circ}\text{C}$  as that for 10049. The diffusion of  $^{40}\text{Ar}^*$  due to solar heating for 10017 is shown, calculated assuming the K/Ar system was reset at 3.03 Ga (C) or 3.56 Ga (D) (symbols and model parameters are the same as in A). (E) Diffusion of  $^{40}\text{Ar}^*$  due to solar heating, calculated assuming the crystallization age is 3.56 Ga (symbols and model parameters are the same as in B). (F) Duration-temperature conditions required to cause  $>95\%$  loss of  $^{40}\text{Ar}^*$  from the most retentive plagioclase domains in 10017 during the proposed 3.0-Ga thermal event (red curve). The dashed blue curve predicts the time required to cool diffusively from an initial temperature,  $T$ , to  $<100^{\circ}\text{C}$  in the center of a 6-m-thick ejecta blanket. The intersection of this curve with the solid curve gives the peak temperature that would explain the Ar data under this scenario. The green dashed line represents the Curie temperature of kamacite ( $780^{\circ}\text{C}$ ).

Our analyses confirm that like other Apollo group A basalts (32), 10049 has a weighted average  $^{40}\text{Ar}/^{39}\text{Ar}$  plateau age of  $3,556 \pm 8$  Ma [uncertainty is 1 SD; uncertainty in the decay constant and age of the fluence monitor is excluded (33)]. However, 10017's  $^{40}\text{Ar}/^{39}\text{Ar}$  plateau age of  $3,037 \pm 7$  Ma is  $\sim 600$  My younger than its crystallization age (34). Our thermochronological calculations suggest that 10017 may have been heated to several hundred  $^{\circ}\text{C}$  at  $\sim 3.05$  Ga. Although this event may have partially remagnetized or demagnetized low blocking temperature grains in this rock (depending on whether a field was present at this time), many of these grains would have subsequently been demagnetized during zero-field residence on the lunar surface over the intervening 3 Ga and during residence in our laboratory's shielded room. As has been inferred for many other Apollo 11 basalts (7, 35), both 10017 and 10049 also apparently experienced modest gas loss due to solar heating over the last  $304.7 \pm 2.0$  Ma and  $17.5 \pm 0.1$  Ma, respectively. In particular, numerical models of simultaneous production and diffusion of both radiogenic  $^{40}\text{Ar}$  and cosmogenic  $^{38}\text{Ar}$  indicate that sample 10049 only experienced temperatures in excess of the ambient crustal conditions because it was exposed near the lunar surface.

### Implications for the Power Source of the Lunar Dynamo

Large impacts have the potential to unlock the Moon from synchronous rotation (36), such that the resulting differential motion between the librating mantle and core could generate a dynamo lasting for up to  $10^7$  y (10). It is estimated that this can only occur for impactors that are larger than that required to produce a crater with a diameter of  $\sim 300$  km (assuming an Earth-Moon distance of 25 Earth radii) (36). The youngest such basin is Orientale, which formed at 3.73 Ga and marks the end of the Early Imbrian epoch (37, 38). Because this event occurred  $\sim 160$  Ma before the Late Imbrian eruption of 10017 and 10049, this likely excludes unlocking from synchronous rotation as a field source at 3.6 Ga.

Smaller impacts that are insufficient to unlock the Moon from synchronous rotation could still generate a mechanical dynamo by inducing longitudinal free librations (10). However, it is estimated that this was only possible while the Earth-Moon separation was  $< \sim 40$  Earth radii. Orbital history models constrained by geological evidence for the past 0.6 Ga (39, 40) suggest that the Earth-Moon separation was 37–44 Earth radii at 3.6 Ga, whereas uniformly scaled models give a range of 47–51 Earth radii (41). Therefore, the conditions for the existence of a libration dynamo might have been met during the eruption of the high-K basalts. Assuming this is the case, it is estimated that for the smallest Earth-Moon separation (37 Earth radii), an impact would have to produce a libration amplitude of at least  $70^{\circ}$  to trigger a libration dynamo (10). Using equations 1 and 6 in ref. 42, we determined the minimum impactor diameter [assuming a spherical bolide with uniform density of  $3,500 \text{ kg}\cdot\text{m}^{-3}$  and a lunar crustal density of  $2,691 \text{ kg}\cdot\text{m}^{-3}$  (43)] required to induce a libration dynamo as a function of impact location colatitude  $\theta$ , impact trajectory inclination relative to the lunar spin axis  $\theta_v$ , impact trajectory declination relative to the impact location  $\phi_v$ , and velocity  $V$  (angles are defined in Fig. 4, *Inset*). Using the crater-scaling equation 5.6 in ref. 44, we calculated the corresponding crater size  $D_{\min}$ . Using the impact velocity probability distribution  $p(V)$  of Le Feuvre and Wieczorek (37), the probability distribution  $p(\theta_v)$  of impact inclinations of Le Feuvre and Wieczorek (45), and the probability distribution of impact geographic colatitude  $p(\theta)$  calculated from the relative cratering rate variations with latitude of Le Feuvre and Wieczorek (45); assuming a uniform distribution for impact declinations  $\phi_v$ ; and ignoring the curvature of impact trajectories and acceleration due to the gravity of the Moon (which would tend to make trajectories more vertical and larger craters, and therefore reduce the effect on librations for a given crater size), we computed the probability

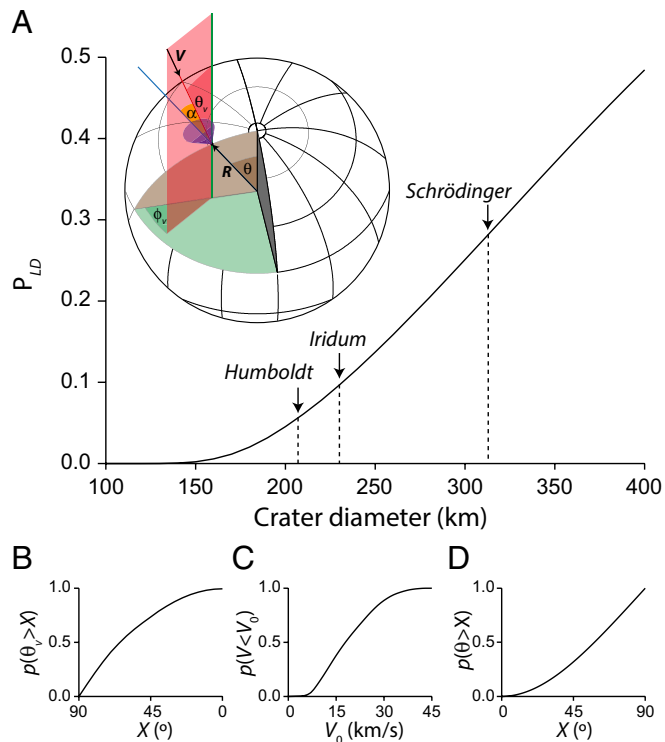


**Fig. 4.** (A) Probability to have induced a libration dynamo as a function of crater diameter. The diameters of the Late Imbrian crater Humboldt and Early Imbrian craters Iridum and Schrödinger are shown. (*Inset*) Impact geometry. The red line is the impact trajectory; the red surface is the plane defined by the impact trajectory and a line parallel to the lunar spin axis at the impact location. The blue line is the local vertical. The purple cone represents trajectories with  $\alpha > 80^{\circ}$ . (B) Cumulative probability distribution for the inclination of the impact trajectory,  $\theta_v$  (45). (C) Cumulative probability distribution for the impact velocity,  $V$  (37). (D) Cumulative probability distribution for the impact location colatitude,  $\theta$  (45).

$P_{LD}$  for an impact that produces a crater with diameter  $D$  to induce a libration dynamo (Fig. 4):

$$P_{LD}(D) = \int \int \int \int \delta(\theta, \theta_v, \phi_v, V) \cdot p(\theta) \cdot p(\theta_v) \cdot p(\phi_v) \cdot p(V) \cdot d\theta \cdot d\theta_v \cdot d\phi_v \cdot dV$$

$$\delta(\theta, \theta_v, \phi_v, V) = \begin{cases} 1 & \text{if } D_{\min}(\theta, \theta_v, \phi_v, V) \leq D \\ 0 & \text{if } D_{\min}(\theta, \theta_v, \phi_v, V) > D \end{cases}$$

where  $\delta$  selects impact parameters that produce craters larger than the threshold value  $D_{\min}$ . Impacts with incidence angles  $\alpha > 80^{\circ}$  [where  $\alpha = \arccos(\mathbf{RV}/R|V|)$ ; angle and vector definitions are provided in Fig. 4, *Inset*] are expected to produce elliptical craters (46). Because no such crater is known to have formed in the Late Imbrian era, we excluded these trajectories. We find that only craters with a diameter  $> \sim 230$  km have a probability to induce a libration dynamo  $> 10\%$  (Fig. 4). All the craters with a diameter  $> 230$  km identified in a recent Lunar Reconnaissance Orbiter survey\* (47) are presented in *SI Appendix, Table S1*. The largest crater identified in the Late Imbrian era is Humboldt (38, 47); its diameter is  $\sim 207$  km, which corresponds to a probability of  $\sim 6\%$  to induce a libration dynamo. The youngest impacts that had

\*Kadish SJ, et al. (2011), A global catalog of large lunar crater ( $\geq 20$  KM) from the Lunar Orbiter Laser Altimeter, 42nd Lunar and Planetary Science Conference (March 7-11, The Woodlands, TX), Abstract 1006.

a significant (>25%) probability to trigger a libration dynamo are the Early Imbrian basins Schrodinger and Orientale (47)\*.

The Late Imbrian 3.56-Ga crystallization age of the high-K basalts means that they are very likely too young to have been magnetized by an impact-driven dynamo. Furthermore, attributing the paleomagnetic records of 76535 at 4.2 Ga (6), 10020 at 3.7 Ga (7), and 10017 and 10049 at 3.6 Ga to an impact-driven dynamo would require a series of transient impact-driven dynamos. The fact that the 10017 and 10049 paleointensities are so similar to one another, as well to those of the 3.72-Ga basalt 10020 (7), argues strongly in favor of a stable lunar dynamo at least between 3.72 and 3.56 Ga. This lifetime is inconsistent with existing models of core convection, which have been unable to power a dynamo unambiguously after 4.1 Ga by thermal convection alone (48). Rather, these results support the possibility of a longer-lived power source for the lunar dynamo, such as precession (9) or thermochemical convection due to core crystallization, although impact-induced core dynamos could have operated earlier in lunar history.

- Fuller M, Cisowski SM (1987) Lunar paleomagnetism. *Geomagnetism*, ed Jacobs JA (Academic, Orlando, FL), pp 307–455, Vol 2.
- Wieczorek MA, et al. (2006) The constitution and structure of the lunar interior. *Reviews in Mineralogy and Geochemistry* 60:221–364.
- Williams JG, Turyshv SG, Boggs DH, Ratcliff JT (2006) Lunar laser ranging science: Gravitational physics and lunar interior and geodesy. *Adv Space Res* 37(1):67–71.
- Weber RC, Lin P-Y, Garnero EJ, Williams Q, Lognonné P (2011) Seismic detection of the lunar core. *Science* 331(6015):309–312.
- Garcia RF, Gagnepain-Beyneix J, Chevrot S, Lognonné P (2011) Very preliminary reference Moon model. *Physics of the Earth and Planetary Interiors* 188(1–2):96–113.
- Garrick-Bethell I, Weiss BP, Shuster DL, Buz J (2009) Early lunar magnetism. *Science* 323(5912):356–359.
- Shea EK, et al. (2012) A long-lived lunar core dynamo. *Science* 335(6067):453–456.
- Williams JG, Boggs DH, Yoder CF, Ratcliff JT, Dickey JO (2001) Lunar rotational dissipation in solid body and molten core. *J Geophys Res* 106(E11):27933–27968.
- Dwyer CA, Stevenson DJ, Nimmo F (2011) A long-lived lunar dynamo driven by continuous mechanical stirring. *Nature* 479(7372):212–214.
- Le Bars M, Wieczorek MA, Karatekin O, Cébron D, Laneuville M (2011) An impact-driven dynamo for the early Moon. *Nature* 479(7372):215–218.
- Fuller M (1998) Lunar magnetism—A retrospective view of the Apollo sample magnetic studies. *Phys Chem Earth* 23(7-8):725–735.
- Runcorn SK (1996) The formation of the lunar core. *Geochim Cosmochim Acta* 60(7):1205–1208.
- Runcorn SK, et al. (1970) Magnetic properties of Apollo 11 lunar samples. *Proceedings of the Apollo 11 Lunar Science Conference held 5–8 January, 1970 in Houston, TX. Volume 3: Physical Properties*, ed AA Levinson (New York, Pergamon Press), pp 2369–2387.
- Stephenson A, Runcorn SK, Collinson DW (1977) Paleointensity estimates from lunar samples 10017 and 10020. *Lunar Science Conference, 8th, (Houston, TX, March 14–18, 1977) Proceedings. Vol 1. (A78-41551 18–91)* (Pergamon Press, Inc., New York), pp 679–687.
- Sugiura N, Strangway DW, Pearce GW (1978) Heating experiments and paleointensity determinations. *Lunar and Planetary Science Conference, 9th (Houston, TX, March 13–17, 1978) Proceedings. Vol 3. (A79-39253 16-91)* (Pergamon Press, Inc., New York), pp 3151–3163.
- Hoffman KA, Baker JR, Banerjee SK (1979) Combining paleointensity methods: A dual-valued determination on lunar sample 10017,135. *Physics of the Earth and Planetary Interiors* 20:317–323.
- Fuller M, Meshkov E, Cisowski CS (1979) On the natural remanent magnetism of certain mare basalts. *Lunar and Planetary Science Conference, 10th, (Houston, TX, March 19–23, 1979). Proceedings. Vol 3. (A80-23677 08-91)* (Pergamon Press, Inc., New York), pp 2211–2233.
- Cournède C, Gattacceca J, Rochette P (2012) Magnetic study of large Apollo samples: Possible evidence for an ancient centered dipolar field on the Moon. *Earth Planet Sci Lett* 331-332:31–42.
- Gattacceca J, Rochette P (2004) Toward a robust normalized magnetic paleointensity method applied to meteorites. *Earth Planet Sci Lett* 227(3–4):377–393.
- Grove TL, Beatty DW (1980) Classification, experimental petrology and possible volcanic histories of the Apollo 11 high-K basalts. *Lunar and Planetary Science Conference, 11th, (Houston, TX, March 17–21, 1980) Proceedings. Vol 1. (A82-22251 09-91)* (Pergamon Press, New York), pp 149–177.
- Beatty DW, Albee AL (1978) Comparative petrology and possible genetic relations among the Apollo 11 basalts. *Lunar and Planetary Science Conference, 9th, Houston, Tex., March 13–17, 1978, Proceedings. Volume 1. (A79-39107 16–91)* (New York, Pergamon Press, Inc.), pp 359–463.
- Garrick-Bethell I, Weiss BP (2010) Kamacite blocking temperatures and applications to lunar magnetism. *Earth Planet Sci Lett* 294(1–2):1–7.
- Dunlop DJ, Ozdemir O (1997) *Rock Magnetism: Fundamentals and Frontiers* (Cambridge Univ Press, New York), p 573.
- Hood LL, Artemieva NA (2008) Antipodal effects of lunar basin-forming impacts: Initial 3D simulations and comparisons with observations. *Icarus* 193(2):485–502.
- Pearce GW, Strangway DW (1972) Cause of secondary magnetization in lunar samples. *Apollo 16 Preliminary Science Report, NASA Special Publication SP-315*, eds Brett R, et al. (National Aeronautics and Space Administration, Houston), pp 7.55–7.58.
- Tauxe L, Staudigel H (2004) Strength of the geomagnetic field in the Cretaceous Normal Superchron: New data from submarine basaltic glass of the Troodos Ophiolite. *Geochemistry, Geophysics, Geosystems*, 10.1029/2003GC000635.
- Gattacceca J, et al. (2010) Can the lunar crust be magnetized by shock: Experimental groundtruth. *Earth Planet Sci Lett* 299(1–2):42–53.
- Weiss BP, et al. (2010) Paleomagnetism of impact spherules from Lunar crater, India and a test for impact-generated fields. *Earth Planet Sci Lett* 298(1–2):66–76.
- Louzada KL, et al. (2008) Paleomagnetism of Lunar impact crater, India. *Earth Planet Sci Lett* 275(3–4):309–319.
- Dunlop DJ, Argyle KS (1997) Thermoremanence, anhyseretic remanence, and susceptibility of submicron magnetites: Nonlinear field dependence and variation in grain size. *J Geophys Res* 102:20199–20210.
- Student (1908) The probable error of a mean. *Biometrika* 6(1):1–25.
- Snyder GA, Lee D-C, Taylor LA, Halliday AN, Jerde EA (1994) Evolution of the upper mantle of the Earth's Moon: Neodymium and strontium isotopic constraints from high-Ti mare basalts. *Geochim Cosmochim Acta* 58(21):4795–4808.
- Renne PR, Balco G, Ludwig K, Mundil R, Min K (2011) Response to the Comment by W. H. Schwarz et al. on “Joint determination of 40K decay constants and 40Ar\*/40K for the Fish Canyon sanidine standard, and improved accuracy for 40Ar/39Ar geochronology” by P. R. Renne et al. (2010). *Geochim Cosmochim Acta* 75(17):5097–5100.
- Papanastassiou DA, Depaolo DJ, Wasserburg GJ (1977) Rb-Sr and Sm-Nd chronology and genealogy of mare basalts from the Sea of Tranquility. *Lunar Science Conference, 8th, (Houston, TX, March 14–18, 1977) Proceedings. Vol 2. (A78-41551 18-91)* (Pergamon Press, Inc., New York), pp 1639–1672.
- Turner G (1971) <sup>40</sup>Ar-<sup>39</sup>Ar ages from the lunar maria. *Earth Planet Sci Lett* 11(1–5):161–191.
- Wieczorek MA, Le Feuvre M (2009) Did a large impact reorient the Moon? *Icarus* 200(2):358–366.
- Le Feuvre M, Wieczorek MA (2011) Nonuniform cratering of the Moon and a revised crater chronology of the inner Solar System. *Icarus* 214(1):1–20.
- Wilhelms DE (1987) *The Geologic History of the Moon* (US Department of the Interior, Washington, DC), p 302.
- Williams GE (2000) Geological constraints on the Precambrian history of Earth's rotation and the Moon's orbit. *Rev Geophys* 38(1):37–59.
- Walker JCG, et al. (1983) Environmental evolution of the Archean-Early Proterozoic Earth. *Earth's Earliest Biosphere: Its Origin and Evolution*, ed Schopf JW (Princeton Univ Press, Princeton), pp 260–290.
- Touma J, Wisdom J (1994) Evolution of the Earth-Moon system. *Astron J* 108(5):1943–1961.
- Peale SJ (1975) Dynamical consequences of meteorite impacts on the Moon. *J Geophys Res* 80(35):4939–4946.
- Huang Q, Wieczorek MA (2012) Density and porosity of the lunar crust from gravity and topography. *J Geophys Res* 117:E05003.1–E05003.9.
- Stöffler D, Ryder G, Ivanov BA, Artemieva NA (2006) Cratering history and lunar chronology. *Reviews in Mineralogy and Geochemistry* 60:519–526.
- Le Feuvre M, Wieczorek MA (2008) Nonuniform cratering of the terrestrial planets. *Icarus* 197(1):291–306.
- Bottke WF, Love SG, Tytell D, Glotch T (2000) Interpreting the elliptical crater populations on Mars, Venus and the Moon. *Icarus* 145(1):108–121.
- Head JW, 3rd, et al. (2010) Global distribution of large lunar craters: Implications for resurfacing and impactor populations. *Science* 329(5998):1504–1507.
- Stegman DR, Jellinek AM, Zatman SA, Baumgardner JR, Richards MA (2003) An early lunar core dynamo driven by thermochemical mantle convection. *Nature* 421(6919):143–146.